Supporting Information

Hydrogen-Bonded Organic Semiconductor Micro- and Nanocrystals: From Colloidal Syntheses to (Opto-)Electronic Devices.

Mykhailo Sytnyk,[§] Eric Daniel Głowacki,[#] Sergii Yakunin,[§] Gundula Voss,[#] Wolfgang Schöfberger,[▽,†] Dominik Kriegner,[§] Julian Stangl,[§] Rinaldo Trotta,[§] Claudia Gollner,[§] Sajjad Tollabimazraehno,[||] Giuseppe Romanazzi,[⊥] Zeynep Bozkurt,[#] Marek Havlicek,[#] Niyazi Serdar Sariciftci,[#] Wolfgang Heiss*[§‡*]

[§]Institute of Semiconductor and Solid State Physics, [#]Linz Institute for Organic Solar Cells (LIOS), Physical Chemistry, [▽]Institute of Organic Chemistry, [||]Zentrum für Oberflächen- und Nanoanalytik, Johannes Kepler University Linz, Altenberger Straße 69, 4040 Linz, Austria.

[⊥] Dipartimento di Ingegneria Civile, Ambientale, del Territorio, Edile e di Chimica (DICATECh), Politecnico di Bari, Via Orabona 4, 70125 Bari, Italy.

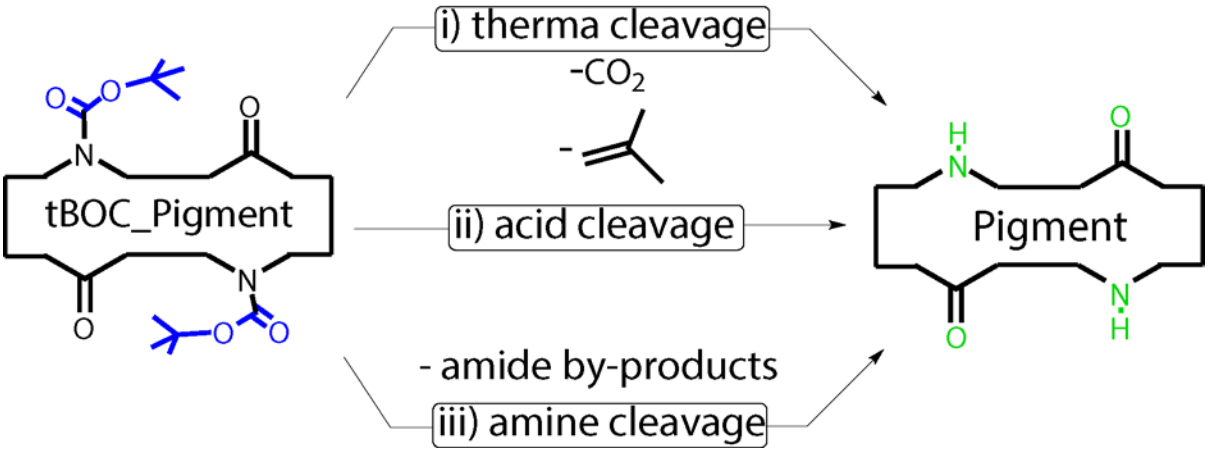

Figure S1. Three different routes were applied in this work for deprotection of latent pigments to crystallize organic pigment micro-nanocrystals in organic solutions.

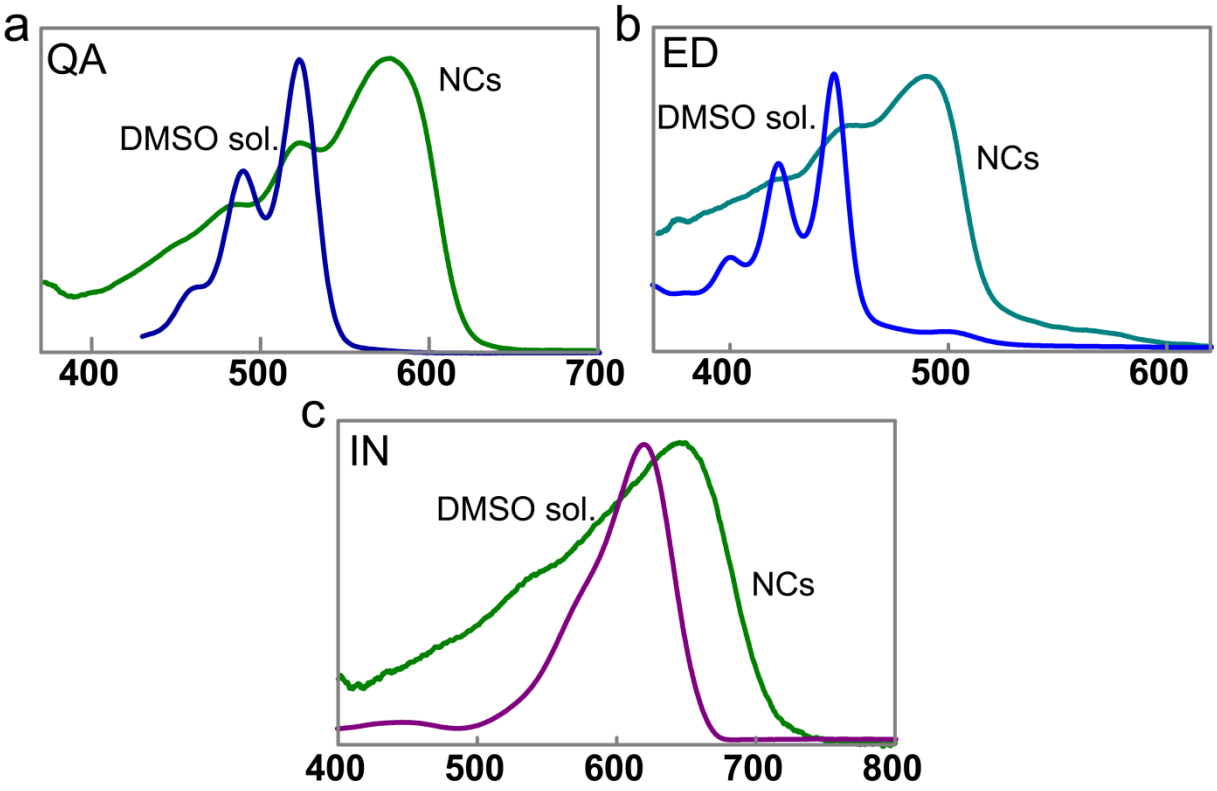

Figure S2. Optical properties of latent pigments versus pigment micronanocrystals. Absorbance spectra of organic pigments dissolved in DMSO and the corresponding micro-nanocrystals (NCs) dispersed in chloroform (QA=quinacridone, ED=epindolidione, IN=indigo).

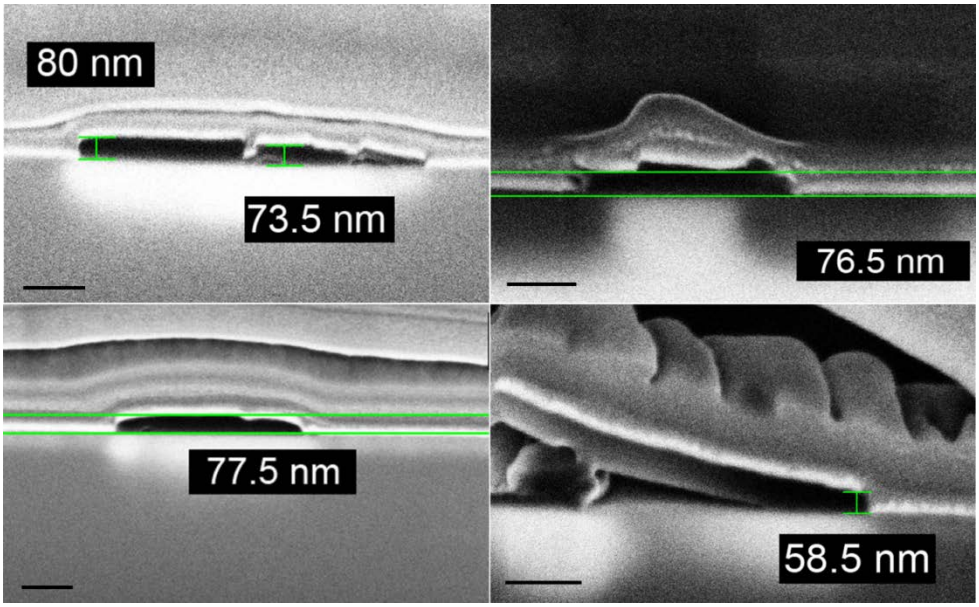

Figure S3. Nanoplatelet thicknesses. Cross sectional scanning electron images of quinacridone nano-platelets with typically thicknesses below 100 nm. The cross sections are prepared by focused ion beam preparation of the nano-platelets covered by a conductive carbon film.

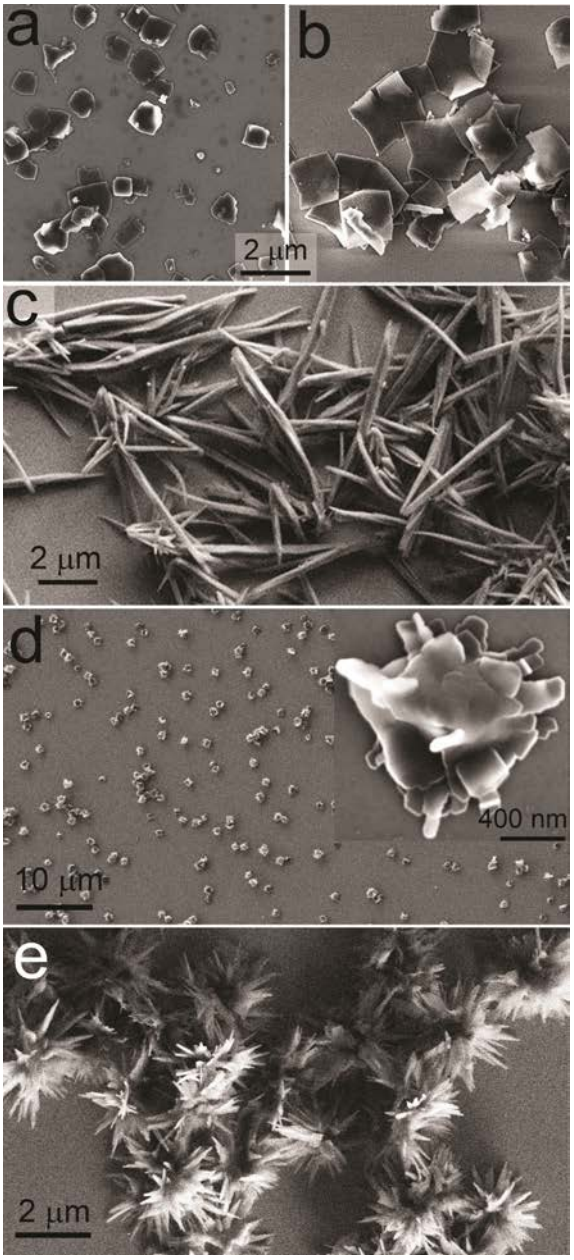

Figure S4. Size and shape controlled quinacridone nanocrystals. (a),(b) By increasing the injection temperature from 280°C to 325 °C the averaged dimensions of the platelet shaped micronanocrystals are increased. (c) Quinacridone micronanocrystals with the shape of rods or needles, synthesized at an injection temperature of 150°C and a growth time of 2 min. (d),(e) Changing the solvent/ligand mixture to pure myristoyl chloride results at a growth temperature of 220°C in irregular structures, whereas the addition of LiCl as catalyst provides regular, star shaped 3-dimensional structure.

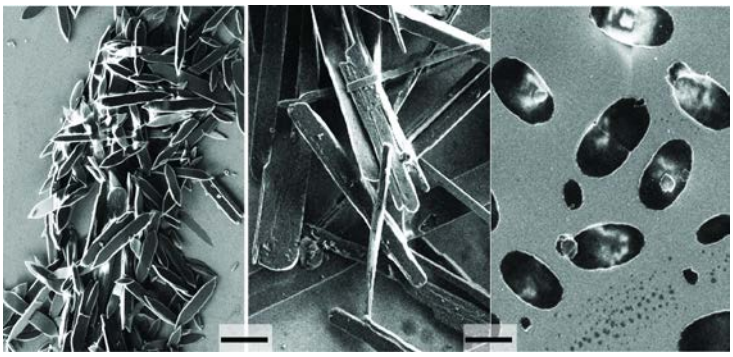

Figure S5 Size controlled platelet shaped indigo micronanocrystals. The size and shape of indigo micronanocrystals depends sensitively on synthetic conditions (Scale bar 5 μm).

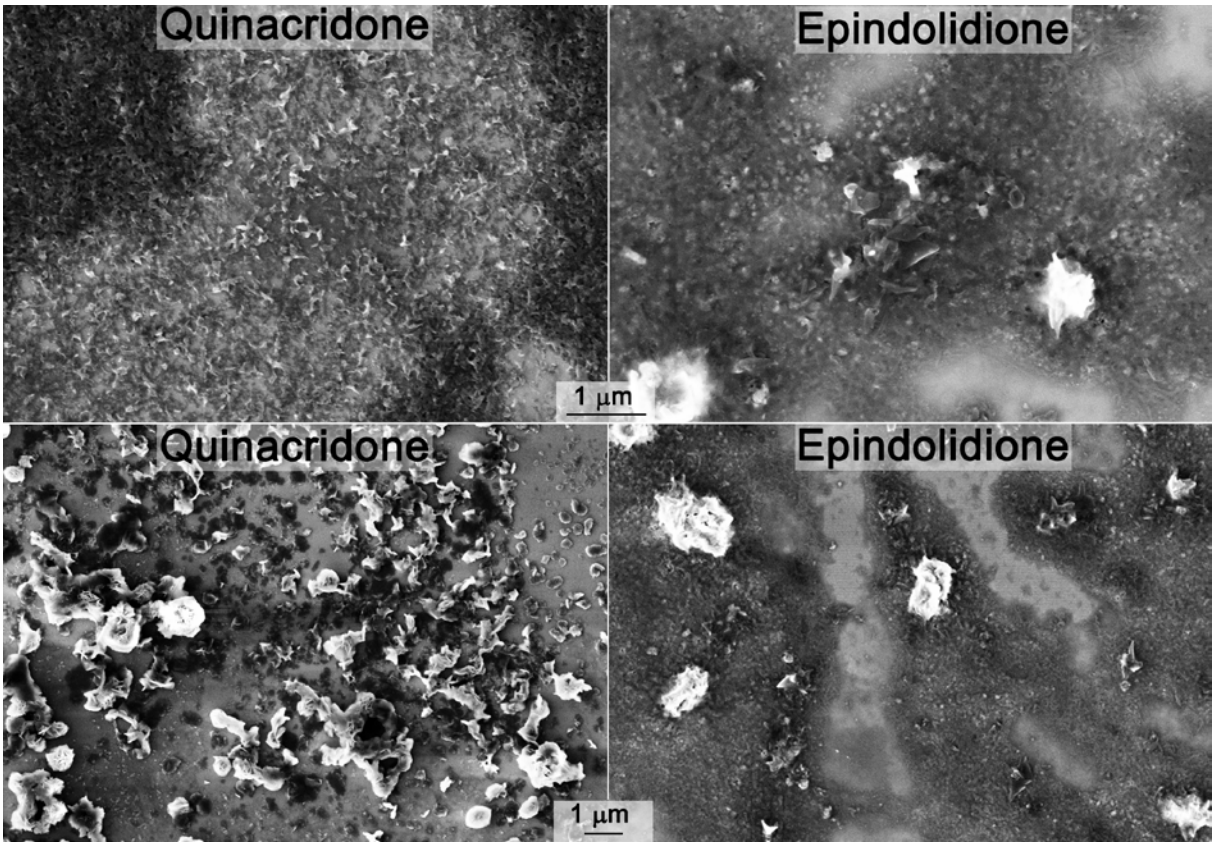

Figure S6. Nanoparticles obtained by the classical precipitation approach. The synthesis was done according to the recipe given by Nakanishi et al. (Novel process for producing pigment nanoparticle, US 2006/0076298 A1, Apr. 13, 2006)

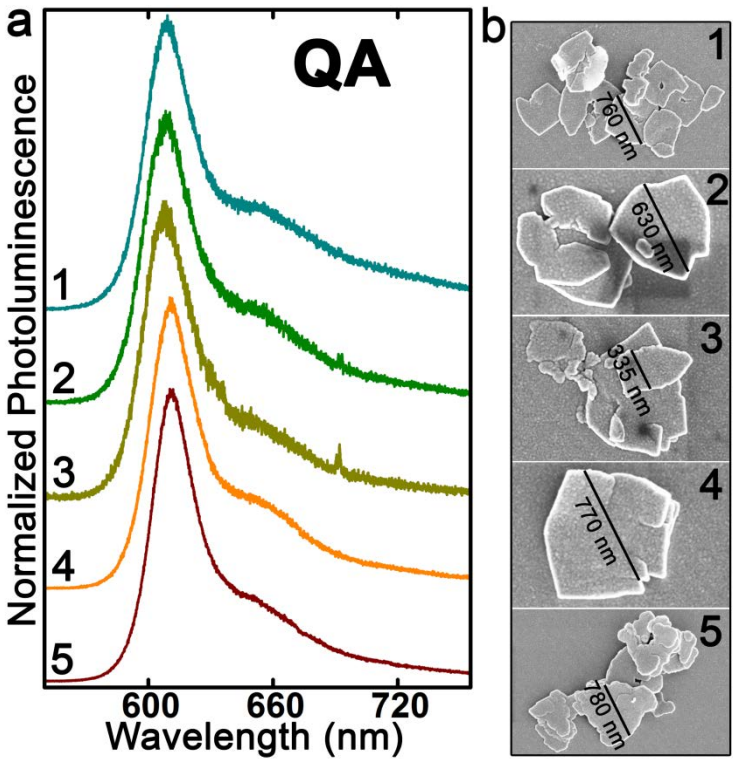

Figure S7. Size independent photoluminescence. (a) Microluminescence spectra of individual, and bunches of a few quinacridone micronanocrystals. (b) Electron micrographs of the very same nanocrystals providing the photoluminescence spectra shown in (a).

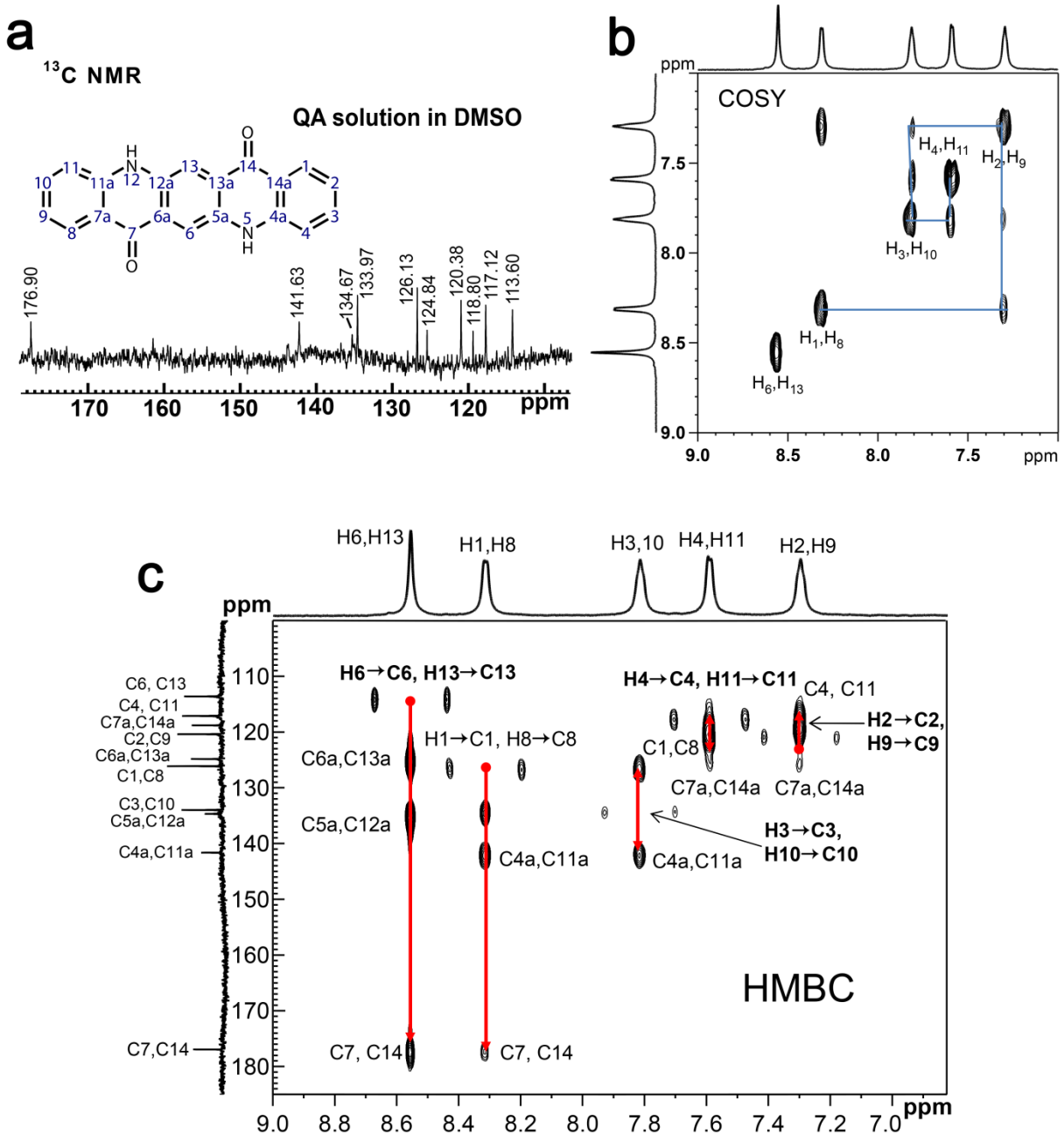

Figure S8. Identification of molecular structure. (a) Solution NMR C-spectrum, obtained for quinacridone monomers dissolved in dimethylsulfoxid (DMSO), assigned to the corresponding atoms. The assignment was enabled by (b), Homonuclear ^{1}H-^{1}H COrrelation SpectroscopY (COSY) and (c) Heteronuclear Single Quantum Coherence (^{1}H-^{13}C HSQC) NMR spectroscopy data.

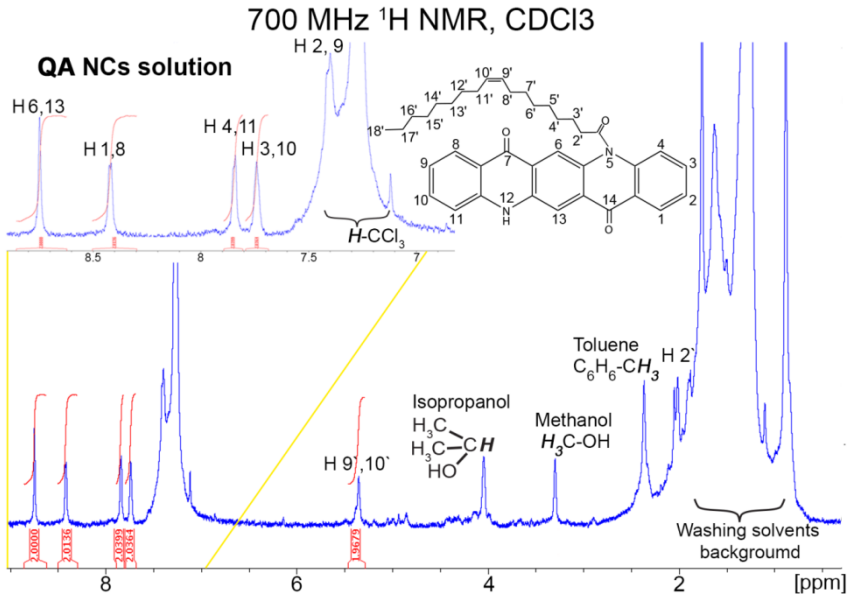

Figure S9. Identification of NMR H-Spectrum. With the help of S5 and data from literature all peaks in the H-spectrum can be assigned to the corresponding atoms of quinacridone or the oleate group of the ligand. In addition residuals of some used solvents are identified.

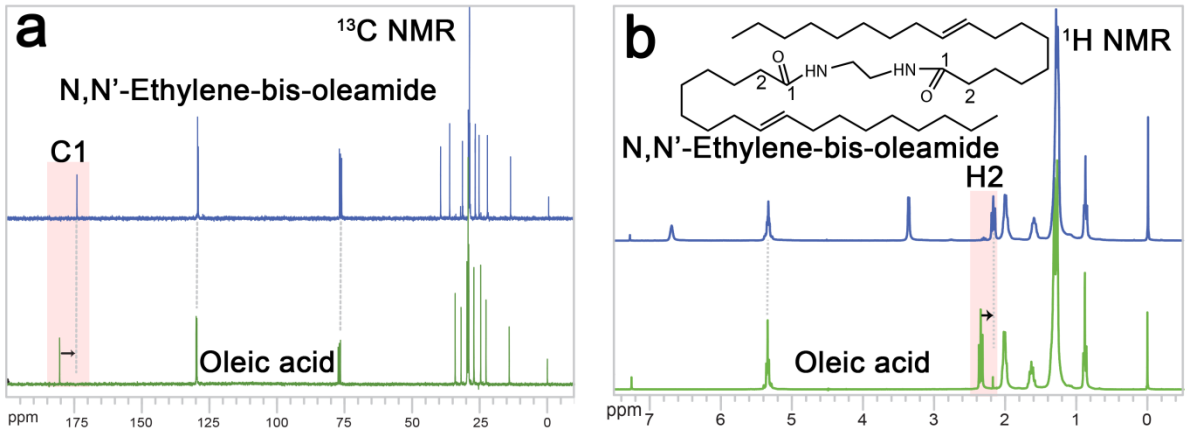

Figure S10. Evidence for ligand attachment. The different positions in the ^{13}C NMR spectra and ^{1}H NMR spectra of oleic acid and N,N´-Ethylene-bis-oleamide observed for the C1 and H2 peaks are characteristic for free oleic acid and oleic acid bound to nitrogen nuclei. The same characteristic peak shifts are observed in the ^{1}H-^{13}C HMBC spectra of **quinacridone micronanocrystals** as compared to that of free oleic acid (Figure 5 of the main text), confirming the ligand attachment.

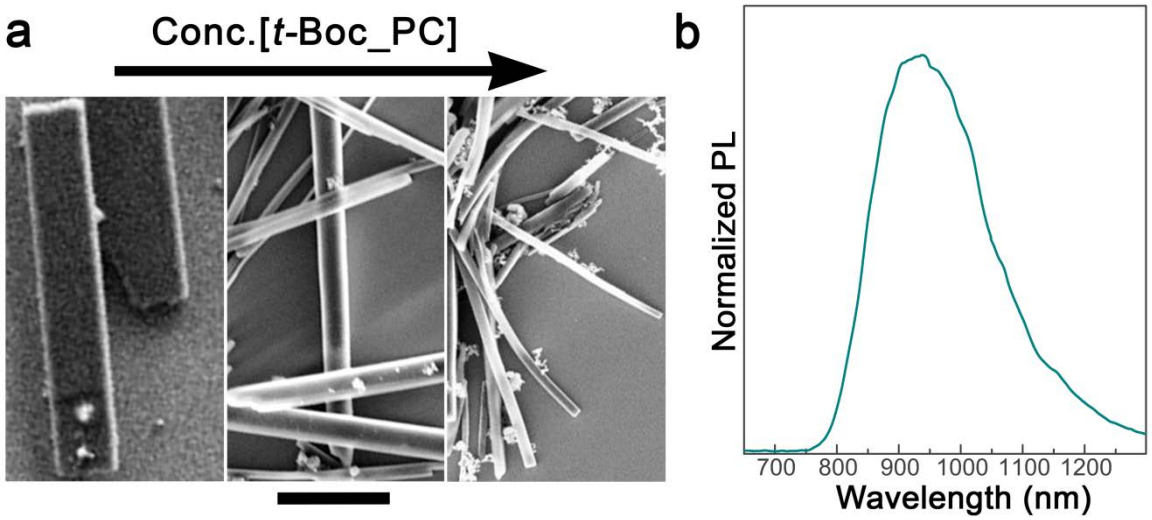

Figure S11. Phthalocyanine micronanocrystals by self decomposition of *t*-BOC-PC. (a) Increasing the concentration of *t*-Boc-phthalocyanine results in smaller lateral dimensions of the rectangular shaped nanocrystals (scale bar: 2 μm). (b) Such micronanocrystals provide luminescence in the near-infrared spectral region.

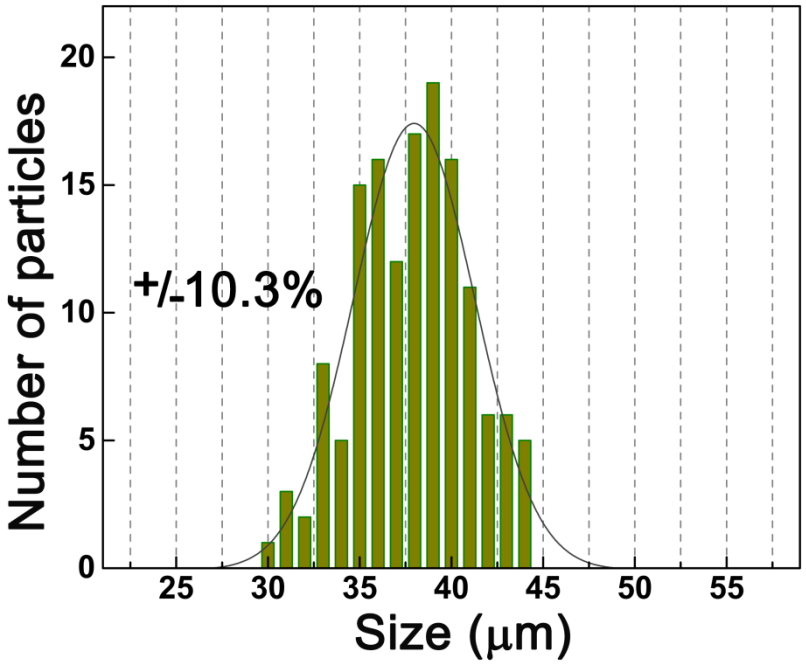

Figure S12. Size dispersion of spherical phthalocyanine nanocrystals. The size dispersion of the 0D nanospheres given in Figure 6(c) of the main text was evaluated from electron microscopy images.

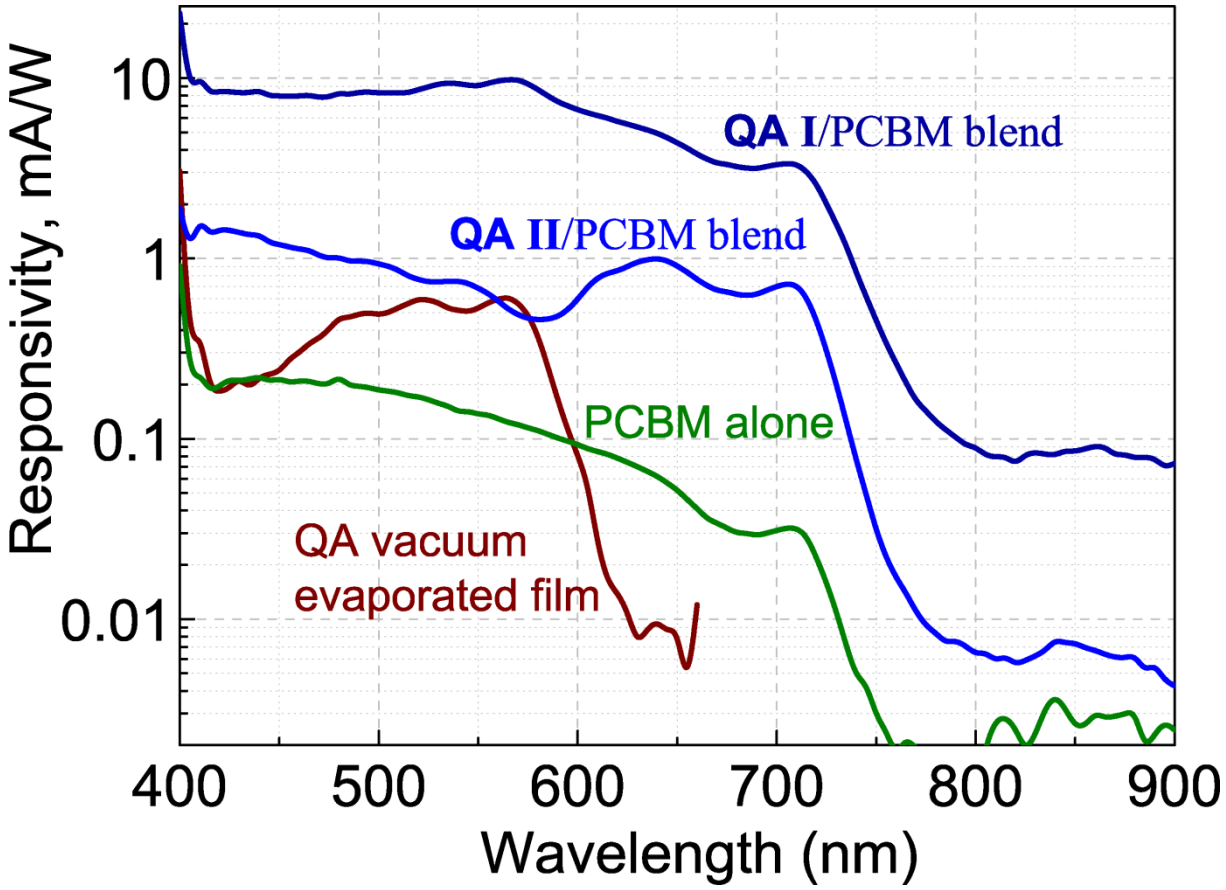

Figure S13. Photoresponse of quinacridone based devices. The response of bulk-heterojunction hybrid blends of quinacridone micronanocrystals with PCBM is superior to that of thermally evaporated films.

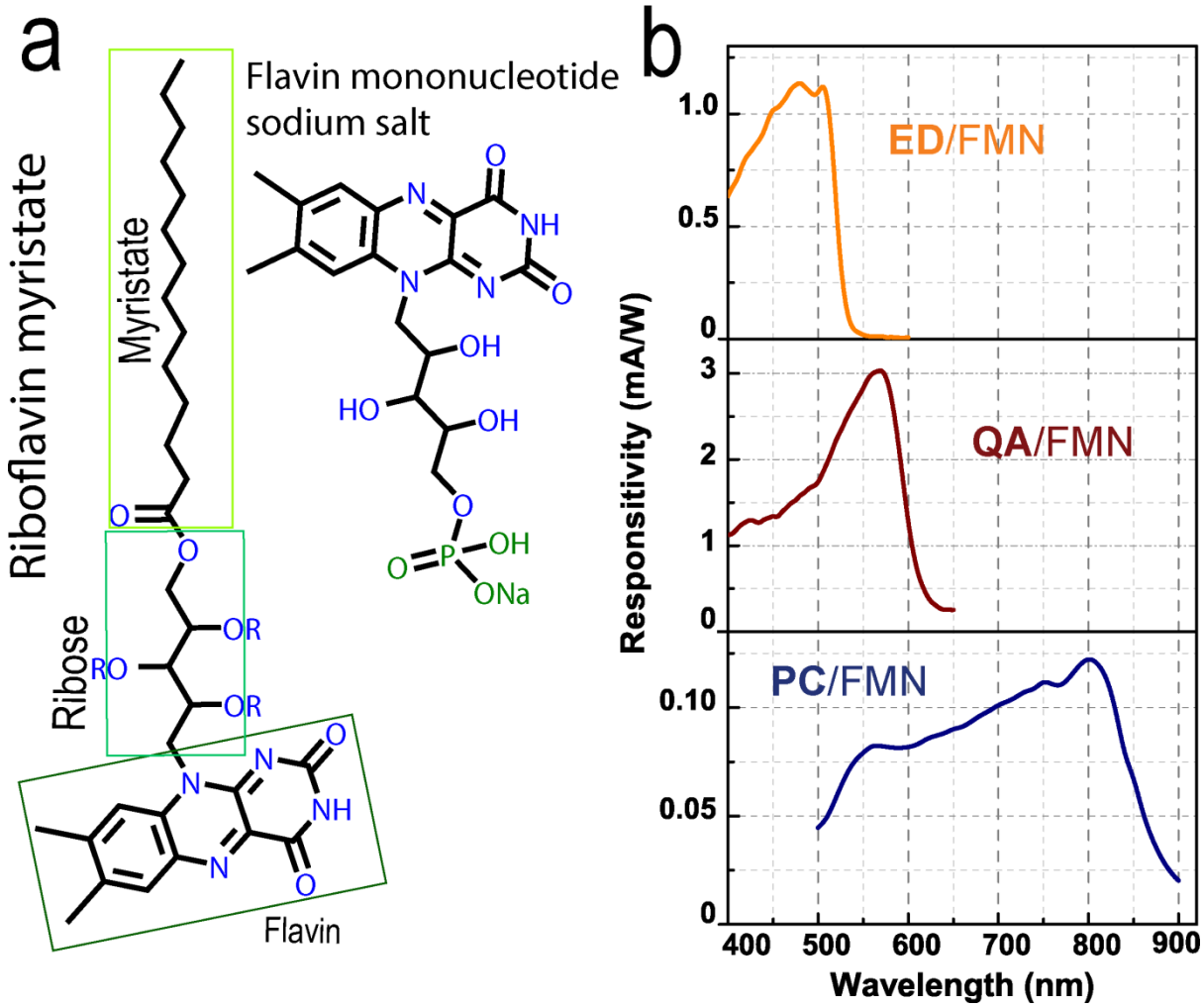

Figure S14. Electron accepting flavin ligands and flavin containing salts. (a) The riboflavin myristate consists of 3 moieties, indicated by coloured frames. Hydrogen bonding to the **quinacridone** surfaces is possible at several sites of the three conjugated rings, marked in blue. The electron accepting properties of flavin enable also photoconductivity in blends of flavin mononucletotide (FMN) sodium salt with various organic pigment micronanocrystals (see (b) ED=epindolidione, QA=quinacridone, PC=phthalocyanine).